PCCP

Specific Zinc Binding to Heliorhodopsin

Journal:	*Physical Chemistry Chemical Physics*
Manuscript ID	CP-ART-10-2022-004718.R1
Article Type:	Paper
Date Submitted by the Author:	15-Dec-2022
Complete List of Authors:	Hashimoto, Masanori; Nagoya Institute of Technology Miyagawa, Koichi; University of Tsukuba, Physics Singh, Manish; Regional Centre for Biotechnology Katayama, Kota; Nagoya Institute of Technology Shoji, Mitsuo; Tsukuba University, Graduate School of Pure and Applied Sciences Furutani, Yuji; Institute for Molecular Science, Department of Life Science and Applied Chemistry Shigeta, Yasuteru; University of Tsukuba, Physics Kandori, Hideki; Nagoya Institute of Technology,

Specific Zinc Binding to Heliorhodopsin

Masanori Hashimoto,[a] Koichi Miyagawa,[b] Manish Singh,[a] Kota Katayama,[a,c,d] Mitsuo Shoji,[*,b,d] Yuji Furutani,[a,c] Yasuteru Shigeta, [b] and Hideki Kandori[*,a,c]

[a]Department of Life Science and Applied Chemistry, Nagoya Institute of Technology, Showa-ku, Nagoya 466-8555, Japan

E-mail: kandori@nitech.ac.jp

[b]Center for Computational Sciences, University of Tsukuba, Tsukuba, Ibaraki 305-8577, Japan

Email: mshoji@ccs.tsukuba.ac.jp

[c]OptoBioTechnology Research Center, Nagoya Institute of Technology, Showa-ku, Nagoya 466-8555, Japan

[d]JST-PRESTO, Kawaguchi, Saitama 332-0012, Japan

Abstract

Heliorhodopsin (HeR), a recently discovered new rhodopsin family, has an inverted membrane topology compared to animal and microbial rhodopsins. The slow photocycle of HeRs suggests a light-sensor function, although the function remains unknown. Although HeRs exhibit no specific binding of monovalent cations or anions, recent ATR-FTIR spectroscopy demonstrated binding of Zn^{2+} to HeR from *Thermoplasmatales archaeon* (TaHeR) and 48C12. Even though ion-specific FTIR spectra were observed for many divalent cations, only helical structural perturbations were observed for Zn^{2+}-binding, suggesting a possible modification of HeR function by Zn^{2+}. The present study showed that Zn^{2+}-binding lowers thermal stability of TaHeR, and slows back proton transfer to the retinal Schiff base (M decay) during its photocycle. Zn^{2+}-binding was similarly observed for TaHeR opsin that lacks the retinal chromophore. We then studied Zn^{2+}-binding site by means of ATR-FTIR spectroscopy of site-directed mutants. Among five and four mutants of His and Asp/Glu, respectively, only E150Q exhibited completely different spectral feature of α-helix (amide-I) in ATR-FTIR spectroscopy, suggesting that E150 is responsible for Zn^{2+}-binding. Molecular dynamics (MD) simulation built a coordination structure of Zn^{2+}-bound TaHeR, where E150 and protein bound water molecules participate direct coordination. It was concluded that the specific binding site of Zn^{2+}

is located at the cytoplasmic side of TaHeR, and Zn^{2+}-binding affects structure and structural dynamics, possibly modifying the unknown function of TaHeR.

Rhodopsins are integral membrane proteins that bind retinal chromophores.[1] In addition to type-1 microbial and type-2 animal rhodopsins, a previously unrecognised diverse family, heliorhodopsins (HeRs), was recently discovered through the use of functional metagenomics.[2,3] HeR 48C12, the first reported HeR, has an inverted membrane topology compared to type-1 and -2 rhodopsins, no ion-transport activity, and its slow photocycle suggests a light-sensor function, although there is currently no information about any interaction partner(s) of HeRs.[2]

Crystal structures of HeR from *Thermoplasmatales archaeon* (TaHeR),[4] and 48C12[5,6] showed that HeRs form a dimer, where a long β-sheet in one molecule covers the extracellular surface of another molecule.[4-6] The structure of the transmembrane region resembles that of type-1 rhodopsins, despite limited sequence homology. The crystal structure of 48C12 at pH 4.3 observed binding of anions such as acetate at the cytoplasmic side.[6] On the other hand, an ATR-FTIR study demonstrated no binding of monovalent cations and anions to TaHeR at physiological pH.[4] Similar results were observed for Co^{2+} and Mg^{2+}, whereas clear binding signals were detected for Zn^{2+}, Cu^{2+}, Ni^{2+}, Cd^{2+}, Mn^{2+} and Ca^{2+}.[7] Among these divalent cations, only Zn^{2+} binding accompanies helical structural perturbation. Therefore, we concluded that Zn^{2+} binds to TaHeR with two modes; specific binding (Kd = 0.2 mM) with helical structural perturbation, and non-specific binding (Kd > 5 mM).[7] Non-specific binding is common for other divalent cations such as Cu^{2+}, Ni^{2+}, Cd^{2+}, Mn^{2+} and Ca^{2+}, while structural changes of α-helix suggests a possible modification of HeR function by Zn^{2+}. Similar results were obtained for HeR 48C12.[7]

Suggested functional correlation of Zn^{2+} binding to HeRs raised various questions. How are static and dynamic molecular properties of HeRs altered by Zn^{2+}? Where is the binding site of Zn^{2+}? In this study, we first compared thermal stability of TaHeR and photocycle dynamics between the presence and absence of Zn^{2+}. We also tested if Zn^{2+} binds or not to the opsin, the protein without the retinal chromophore. We then studied the binding site of Zn^{2+}, especially

specific binding. Binding of Zn^{2+} did not change the color of TaHeR,[7] suggesting that the Zn^{2+} binding site is distant from the retinal chromophore. From the ATR-FTIR spectra of Zn^{2+} binding to HeRs, tetrahedral coordination with carboxylate and imidazole groups was suggested. Figure 1 shows that TaHeR contains two aspartates, seven glutamates, and five histidines. If carboxylate and histidine both participate in the coordination of Zn^{2+}, then the binding site must be in the cytoplasmic region since histidines are not present at the extracellular surface. Among the five histidines, H23 and H82 are located near the retinal chromophore,[4-6] whose mutations induce a change in colors.[8] As Zn^{2+}-binding does not alter the color of TaHeR, H23 and H82 may not be the candidates. In this study, we attempted to identify the binding site of Zn^{2+} by systematic mutation. We mutated all histidine residues including H23 and H82. Among nine carboxylates, E108 is the Schiff base counterion, whose mutation is sensitive to color.[8-10] Therefore, we selected two carboxylates at the cytoplasmic side (E150 and E227), and at the extracellular side (D128 and E186). Among five and four mutants of His and Asp/Glu, respectively, only E150Q exhibited completely different spectral feature of α-helix (amide-I). We thus concluded that E150 coordinates Zn^{2+} upon its specific binding. The binding mode and influence of protein structure were further examined by molecular dynamics (MD) simulation.

Results and Discussion

Static and dynamic properties of TaHeR in the presence of zinc.

Figure S1 compared thermal stability of solubilized TaHeR molecule (0.1 % DDM) with and without divalent cations. In the absence of divalent cations, absorption spectra of TaHeR (λ_{max} = 542 nm) are identical at 20-50 °C, but the visible absorption at 500-600 nm diminishes at >70 °C, and UV absorption at 300-400 nm increases (Figure S1a). This suggests thermal denaturation of TaHeR, and Tm was determined to be 79.5 °C (Figure 2). Temperature dependence of absorption spectra of TaHeR was similar in the presence of 0.5 mM Mg^{2+} (Figure S1b), whose Tm was determined to be 79.2 °C (Figure 2). In contrast, temperature-dependent

spectral feature was highly different in the presence of 0.5 mM Zn^{2+}, where decrease of visible absorption took place at lower temperatures (Figure S1c). From Figure 2, Tm value was determined to be 71.1 ^{o}C. This result indicates that Zn^{2+}-bound TaHeR is more unstable than the unbound form.

We then measured photocycle of TaHeR in the absence and presence of 0.5 mM Zn^{2+}. Figure 3 shows appearance of similar intermediate states; K is converted to M at 10^{-6}-10^{-5} sec, M is converted to O at 10^{-4}-10^{-3} sec, and O is reverted to the original state in the time scale of 10 sec. Nevertheless, we observed clear kinetic difference, especially on the decay of the M intermediate. The observed time constant of the M decay was 0.15 and 0.44 ms in the absence and presence of Zn^{2+}, respectively, indicating the retarded reprotonation of the Schiff base for the Zn^{2+}-bound TaHeR. Proton accepting group (PAG) in the M intermediate of TaHeR has not been identified.[2,4] Protein bound water cluster is the strong candidate of PAG,[4-6] whereas there is no experimental evidence. The present result suggests that Zn^{2+} stabilizes protonated PAG in the M intermediate. On the other hand, there was little influence of Zn^{2+} for the formation of the M intermediate and the decay of the O intermediate.

Difference FTIR spectra of TaHeR upon Zn^{2+} binding.

The results of Figures 2 and 3 clearly showed the effect of Zn^{2+} binding on thermal stability and photochemistry of TaHeR, respectively, where the samples were solubilized by detergent (0.1 % DDM). To gain structural insights, we next applied ATR-FTIR spectroscopy. Stimulus-induced difference ATR-FTIR spectra provide vibrational information upon structural changes of protein to stimuli, which is not only light, but also binding of ions and ligands.[11] By this method, we studied molecular mechanism of ion bindings to rhodopsins,[4,7,12-20] stator complex of flagellar motor,[21,22] V-type ATPase,[23,24] KcsA potassium channel,[25,26] voltage-gated proton channel,[27] and sodium-calcium exchanger,[28] as well as ligand bindings to peptide transporter,[29] and M2 muscarinic acetylcholine receptor.[30-32] In the measurements, purified proteins in detergent are reconstituted into lipids, whose protein:lipid molar ratio is from 1:20 to 1:50. In the previous study, however, we found that the reconstitued sample with a protein:lipid molar ratio of 1:20 exhibits significant protein-lipid shrinkage upon binding of divalent cations, so that accurate difference FTIR spectra were not obtained.[7] In contrast, we were able to obtain reproducible cation-binding difference FTIR spectra if lipids were not added. We interpret that TaHeR molecules are surrounded by endogenous lipids upon removal of detergent by Bio-Beads.

In this study, we first examined whether Zn^{2+} binds to the opsin of TaHeR, the apo-protein without retinal. We prepared TaHeR opsin according to the same procedure, but without adding all-trans retinal. Figure S2 compared absolute absorption spectra of TaHeR and TaHeR opsin, both of which were prepared in the absence of additional lipids. Vibrational bands at ~1740 cm^{-1} mainly originate from ester C=O stretches, and thus a marker band of lipids. Presence of this peak for TaHeR (black line in Figure S2) indicates that TaHeR molecules are surrounded by endogenous lipids. This peak is smaller in TaHeR opsin than that in TaHeR, suggesting that lipid contents are smaller in TaHeR opsin sample. Nevertheless, very similar amide-I (1654 cm^{-1}) and -II (1544 cm^{-1}) bands implicate that TaHeR opsin is properly folded as well as TaHeR.

Figure 4 compares the difference ATR-FTIR spectra, where positive and negative signals correspond to the presence and absence of Zn^{2+}, respectively. As His_6-tag was not removed, the difference spectra contain the signals of Zn^{2+} binding to His_6-tag. Nevertheless, similar spectral feature indicates Zn^{2+} binding to TaHeR opsin, as well as retinal-bound TaHeR. In particular, similar spectral feature in the amide-I region implicates the existence of the specific binding of Zn^{2+} to TaHeR opsin. It should be noted that the negative and positive peaks in amide-I were upshifted by 2 and 11 cm^{-1}, respectively. This suggests that binding site of Zn^{2+} and helical structural changes upon Zn^{2+} binding are similar between the presence and absence of the chromophore retinal, but folded protein structure is somehow loosen in TaHeR opsin.

We then measured Zn^{2+} binding to various mutants of TaHeR, which were prepared by the same methods for the wild-type TaHeR. Figure S3 compared absolute absorption spectra of TaHeR mutants. Ester C=O stretches at ~1740 cm^{-1} are smaller in all mutants than that of the wild type, suggesting that lipid contents are smaller in the mutant samples, but very similar amide-I (1655 cm^{-1}) and -II (1544 cm^{-1}) bands suggest that all mutants are properly folded as well as the wild type. In the present study, we did not remove His_6-tag, so that the difference spectra possibly contain the signals of Zn^{2+} binding to His_6-tag. Figure S4 compares the difference spectra of the wild-type TaHeR with and without His_6-tag, where sharp peak at 1116 cm^{-1} is characteristic of the Zn^{2+} binding to His_6-tag. Figure 5 shows essentially similar difference spectra for five histidine mutants (H23F, H82F, H100F, H152F, and H225F), and four carboxylate mutants (D128N, E150Q, E186Q, and E227Q), to that of the wild type (black line). This suggests similar spectral feature of Zn^{2+} binding to the non-specific binding site and His_6-tag. The specific binding of Zn^{2+} to TaHeR can be seen by the amide-I bands, where the 1659 (+)/1649 (-) cm^{-1} of the wild-type TaHeR (black line) shows helical structural perturbation by weakening the hydrogen bond upon Zn^{2+} binding.[7] Most of the obtained spectra exhibit

similar spectral feature with the up-shifted frequencies like TaHeR opsin (Figure 4). Nevertheless, only one exception was seen for E150Q. In case of E150Q, we observed spectral down-shift in the amide-I region. It should be noted that the spectra of amide-I region in D128N, E186Q, and E227Q also differ from that of the wild type, but they exhibit spectral up-shift in the amide-I region as well as the wild type and the wild-type opsin (Figure 4). The unusual spectral feature only observed for E150Q strongly suggests that E150 is related to the specific binding of Zn^{2+}, and the most straightforward interpretation is that E150 constitutes the coordination group of Zn^{2+} binding in TaHeR.

In addition to the amide-I bands, the ATR-FTIR spectra of the wild-type TaHeR contain the bands at 1600-1550, 1430-1400, and 1150-1000 cm^{-1}, characteristic for carboxylate COO^- antisymmetric vibration, carboxylate COO^- symmetric vibration, and vibrations of the histidine imidazole ring, respectively (Figure S4). Characteristic vibrations of carboxylate and histidine strongly suggest the involvement of Asp/Glu and His for the binding of Zn^{2+} to TaHeR, and the present mutation study provided the experimental support for E150 as the binding site. No clear reduction of carboxylate COO^- antisymmetric and symmetric vibrations should be noted for E150Q (Figure 5) despite the removal of the COO^- group. Non-specific binding of Zn^{2+} to carboxylates may be predominant in these bands. Zn^{2+} binding near E150 is consistent with the observation of the spectral changes in the histidine imidazole ring, as His is located only in the cytoplasmic side (Figure 1). However, all histidine mutants exhibited similar amide-I bands to those of the wild type (Figure 5). This suggests that histidine does not constitute the direct coordination site, but Zn^{2+} binding alters the environment of His.

Upon binding of Zn^{2+}, carboxylate COO^- antisymmetric and symmetric vibrations appear at 1602 and 1421 cm^{-1}, respectively (Figure S4), and the frequency separation (181 cm^{-1}) became wider than that of the Zn^{2+}-free form (151 cm^{-1}). This suggests that Zn^{2+} is coordinated by the anionic carboxylate with a monodentate or, possibly, a pseudobridging mode.[27,33] No clear signal at 1800-1700 cm^{-1} implies that involvement of the protonated carboxylic acid in the Zn^{2+}-binding can be excluded under the present experimental conditions. We next examined the structural changes of TaHeR upon Zn^{2+} binding to E150 by means of molecular dynamics simulation.

MD simulation of Zn^{2+} binding to TaHeR.

MD simulation clearly indicated the structural changes of TaHeR due to the Zn^{2+} coordination to E150 especially in the TM4 and TM5 helices. Figure 6A shows the overlayed representative structure of TaHeR and Zn^{2+}-binding TaHeR of monomer B. Note that a little difference was found for monomer A. This point will be discussed later. For TaHeR, the helix structure of TM4 was kept near the loop region connecting to TM5. On the other hand, the helix structure of Zn^{2+}-bound TaHeR was partly undone by 1 turn including Zn^{2+}-binding E150 compared with TaHeR. In order to quantify the degree of the helices, Figures 6B and C show the population of the alpha-helix and 3-10 helix structures based on the DSSP method.[34] In the case of Zn^{2+}-bound TaHeR, the alpha-helix population was rapidly dropped around E150 to T156 region compare with TaHeR (Figure 6B). The 3-10 helix character was observed around E150 to T156 for TaHeR, while the 3-10 helix population was disappeared in the same region for Zn^{2+}-bound TaHeR (see Figure 6C). These features are consistent with the ATR-FTIR experiments, where the amide-I vibrations were modulated owing to the Zn^{2+}-binding. This structure change was caused by the exposure of E150 from the inside of the helix interface to the bulk water owing to the coordination to the Zn^{2+} ion. In TaHeR, E150 formed a hydrogen bond with R105 in TM3, which had a tight hydrogen-bonding network including E227 in TM7 and W106 (Figure 6D). On the other hand, in Zn^{2+}-bound TaHeR, R105 formed hydrogen bonds with E227 and E108, and E150 was separated from the hydrogen bonding network (Figure 6E). Since E150 tied TM4 to TM3 in TaHeR, TM4 structure was relaxed without the hydrogen bond to R105 in TM3, resulting in the partial collapse of the helix region.

The structural changes around TM4 further cause the change in the accessibility of water molecules inside the protein. In TaHeR, a water cluster is located at the region surrounded by

TM1, TM2, TM3, and TM7. In Zn^{2+}-bound TaHeR, bulk water molecules can enter a space among TM3, TM4, TM5, and TM6 and sometimes exchange with the water molecules in the water cluster (see movie file in Supporting Information). This might result in the change of the surrounding environment of the Schiff base. In Figure 7, the hydrogen-bonding network nearby the retinal Schiff base is illustrated. As can be seen in these figures, the hydrogen-bonding networks are different from each other. For TaHeR, the retinal Schiff base formed a hydrogen bond with E108 (Figure 7A), while for Zn^{2+}-bound TaHeR, it formed a hydrogen bond with a water molecule (Figure 7B). This change may affect the reprotonation of the Schiff base for Zn^{2+}-bound TaHeR as described before in relation to the observed time constant of the M decay. The leak of the water molecules may also be related to the stability of the protein structures of Zn^{2+}-bound TaHeR. As the temperature of the system increases, water molecules often invade into inside the helix bundle and nearby the Shiff base, resulting in the less thermal stability.

Figures S5A and B show the C_α root-mean-square deviation (C_α-RMSD) values of 3 μs MD simulations. For TaHeR, there was a small difference in C_α-RMSD values between the two monomer units. Their behavior is consistent with the overall C_α-RMSD value. However, for Zn^{2+}-bound TaHeR, there was a gap between C_α-RMSD values of these monomers despite the homodimer. C_α-RMSD value of monomer A was less than that of monomer B. This asymmetric behavior was also clearly found in the C_α root-mean-square fluctuation (C_α-RMSF) values as illustrated in Figures S5C. C_α-RMSF of the monomer B in Zn^{2+}-bound TaHeR became large in two regions of [90-105] and [205-230], which involve TM3 and TM7, respectively. These large fluctuations originated from the lack of the tight hydrogen-bonding network among E150-R105-E227 as found in TaHeR. When E150 bounded to Zn^{2+}, the packing of TM3, TM4, TM7 was loosened, and then the amino-acid residues in TM3 and TM7 can move to fluctuate. Note here that the asymmetric behavior was also found for C_α-RMSF of the monomer A in TaHeR, though the relative magnitude was less compared to C_α-RMSF of the monomer B in Zn^{2+}-bound TaHeR. It is quite interesting that the degree of the asymmetry was enhanced by the Zn^{2+}-

binding. Even though the asymmetric behavior might depend on the initial structures, we did not observe the alternation of the asymmetry within relatively long-time 3μs MD simulation. Since the biological role of the Zn^{2+}-binding is still unknown, it is not confirmed that the asymmetry of the response to the Zn^{2+}-binding has physical or biological meaning. In future work, we'll explore the meaning of Zn^{2+}-binding and the selectivity of Zn^{2+} among several metal cations.

Zn^{2+} binding site to TaHeR.

Based on the present experimental and computational results, we propose that the specific binding site of Zn^{2+} is located at the cytoplasmic side of TaHeR, where E150 directly coordinates Zn^{2+}. On the other hand, the present MD simulation based on the X-ray structure implicates no direct coordination of His to Zn^{2+}, and the remaining coordination groups are likely to be protein bound water molecules. One experimental support of the His coordination was the spectral resemblance between TaHeR and the voltage-gated proton channel (Hv1/VSOP), the latter of which is inhibited by Zn^{2+}. In Hv1/VSOP, Zn^{2+} is coordinated by a tetrahedral geometry with ligands of carboxylate and imidazole groups in addition to a water molecule.[27] However, as suggested by the present MD simulation, it is likely that His alters hydrogen-bonding network upon Zn^{2+} binding, rather than direct coordination. The binding site is considerably distant from the retinal chromophore, being consistent with no color change of TaHeR upon Zn^{2+} binding,[7] and similar binding to TaHeR opsin (Figure 4). MD simulation clearly indicated the structural changes of TaHeR due to the Zn^{2+}. Interestingly, MD simulation showed substantial relocation of hydrogen-bonding networks, but Zn^{2+} binding never alters visible absorption (Figure S1).[7] In this regard, identical absorption of the E108D mutant with that of the wild type may be noted,[9] whose mechanism was discussed based on the crystal

structure.[10] Effect of changes in hydrogen-bonding networks on color tuning will be studied by quantum-chemical calculations in future.

The crystal structure of HeR 48C12 at pH 4.3 observed binding of acetate at the cytoplasmic side.[6] As HeR 48C12 also binds Zn^{2+} specifically,[7] possible link of these binding sites is intriguing. Corresponding glutamate in HeR 48C12 is E149, and according to the crystal structure, E149 does not constitute the acetate binding site.[6] It should be however noted that the cytoplasmic domain of HeRs is comprised of water-containing hydrogen-bonding network.[4-6] Such hydrogen-bonding network is able to accommodate various ions such as Zn^{2+} and acetate.

Upon illumination of HeRs, the M intermediate is formed with the deprotonated Schiff base, whose proton acceptor has not been identified.[2,4] Protein bound water cluster is the strong candidate of the proton acceptor,[4-6] and the present flash photolysis results showed that Zn^{2+} does not affect proton release from the Schiff base (M rise), but slows back proton transfer to the Schiff base (M decay) (Figure 3). This suggests that Zn^{2+} stabilizes the proton-containing hydrogen-bonding network. Zn^{2+} does not affect the decay of the O intermediate (Figure 3), suggesting that the event does not include the region of Zn^{2+} binding.

Conclusions

HeRs exhibit no specific binding of monovalent cations or anions,[4] but recent ATR-FTIR spectroscopy demonstrated binding of Zn^{2+} to HeR from *Thermoplasmatales archaeon* (TaHeR) and 48C12.[7] Here we showed that Zn^{2+}-binding lowers thermal stability of TaHeR, and slows back proton transfer to the retinal Schiff base (M decay) during its photocycle. ATR-FTIR spectroscopy revealed that Zn^{2+}-binding was similarly observed for TaHeR opsin that lacks the retinal chromophore. ATR-FTIR spectroscopy of site-directed mutants suggests that E150 is responsible for Zn^{2+}-binding. Molecular dynamics (MD) simulation built a coordination structure of Zn^{2+}-bound TaHeR, where E150 and protein bound water molecules participate direct coordination. The specific binding site of Zn^{2+} is thus located at the cytoplasmic side of TaHeR, and Zn^{2+}-binding affects structure and structural dynamics,

possibly modifying the unknown function of TaHeR. Functional role of Zn^{2+} binding is now intriguing. If the function of TaHeR is affected by Zn^{2+} binding, TaHeR probably senses intracellular Zn^{2+} concentration, as the Zn^{2+} binding site is located at the cytoplasmic side of membrane.

Although function of HeRs has been fully unknown, we recently reported that a viral HeR from *Emiliania huxleyi* virus 202 (V2HeR3) is a light-activated proton transporter.[35] Three environmental viral HeRs from the same group as well as a more distantly related HeR exhibited similar proton-transport activity, indicating that HeR functions might be diverse similarly to type-1 microbial rhodopsins. In addition, regulation of glutamine synthetase and photolyase by HeRs from Actinobacteria bacterium and Trichococcus flocculiformis, respectively, were recently reported.[36,37] Further experimental and theoretical study will lead to better understanding of structure and function of HeRs, which deepen our knowledge of rhodopsins.[1,38]

Methods

Sample preparation.

The wild-type and mutant TaHeR proteins with an N-terminal His_6-tag were prepared as reported previously.[4,7] Although the construct additionally contained a thrombin cleavage site after the N- terminal His_6-tag, we performed all experiments without cleaving the site in the present study. Briefly, the proteins were expressed in *Escherichia coli* strain C43 (DE3), and cells were disrupted by passage through a French press (Ohtake), following ultracentrifuged for 125,000 × g, 1 hour at 4 °C to obtain membrane fraction. The lysed membranes were solubilized with a buffer of 50 mM MES (pH 6.5), 300 mM NaCl, 5 mM imidazole, and 2 % (w/v) n-dodecyl-*β*-D-maltopyranoside (DDM; anatrace). The supernatant was isolated by ultracentrifugation for 1 hour at 140,000 × g and incubated with Co^{2+}-NTA Sepharose Superflow resin (QIAGEN). After binding, the resin was washed with Co^{2+}-NTA wash buffer: 50 mM MES (pH 6.0), 300 mM NaCl, 5 mM imidazole, and 0.1 % DDM. The protein was then eluted with Co^{2+}-NTA elution buffer: 50 mM MES (pH 6.0), 300 mM NaCl, 500 mM imidazole, and 0.1 % DDM, and the collected fractions were dialyzed against a buffer containing 50 mM

HEPES (pH 7.0), 100 mM NaCl, and 0.1 % DDM. Detergent in the purified TaHeR opsin was removed by using Bio-Beads (SM-2, Bio-Rad) for further ATR-FTIR spectroscopy.

The wild-type TaHeR opsin with an N-terminal His_6-tag was overexpressed in *Escherichia coli* C43 (DE3) strain as described previously[4] except that all-*trans* retinal was not supplemented in the culture to produce TaHeR opsin. The other sample preparation methods were identical to those of the wild-type TaHeR above.

Thermal stability measurements

The thermal stability curves of the TaHeR were measured by monitoring absorption at 542 nm in absence or presence (Zn^{2+} and Mg^{2+}; 0.5 mM conc.) using a UV-Vis spectrophotometer (V650, Varian, Japan). Typically, the measurements were performed in a buffer containing HEPES 50 mM, NaCl 100 mM, DDM 0.1%, pH 7.0) with a sample of optical density of the 0.4 at 542 nm. Desired, sample was heated at rate of 1°C min^{-1} from 20°C to 90°C using the cuvette sealed with adhesive sheet to prevent evaporation in an external Peltier thermostatted single cuvette holder. The sample was kept at desired temperature (20, 25, 30, 35, 40, 45, 50, 55, 60, 65, 70, 75, 80, 85 and 90°C) for 5 min, before measuring the absolute absorption spectra. The decrease in optical density at 542 nm (which correspond to retinal covalently-bound opsin) due to heating was fitted to sigmodal function to get the melting temperature (T_m, mid-point of the transition state).

Laser flash photolysis

The time-evolution of the transient absorption changes of photo-excited TaHeR was observed as described previously.[2,4] For TaHeR, the purified protein was resuspended in a buffer containing 50 mM Tris–HCl (pH 8.0), 100 mM NaCl and 0.1 % DDM. TaHeR were reconstituted into a mixture of POPE and POPG (molar ratio = 3:1) with a protein-to-lipid molar ratio of 1:50 where DDM was removed with BioBeads (SM-2, Bio-Rad). For TaHeR, the sample solution was placed in a quartz cuvette and was excited with a beam of second harmonics of a nanosecond pulsed Nd^{3+}: YAG laser (λ = 532 nm INDI40, Spectra-Physics). The excitation laser power was 3 mJ/pulse. The intensities of the transmitted probe light from a Xe arc lamp (L8004, Hamamatsu Photonics, Japan) were measured before and after laser excitation with an ICCD linear array detector (C8808-01, Hamamatsu, Japan), and transient absorption spectra were obtained by calculating the ratio between them. 30-50 identical spectra were averaged. To obtain the detailed time evolution of the transient absorption change after photoexcitation, the change in the intensity of monochromated output of a Xe arc lamp (L9289-

01, Hamamatsu Photonics, Japan) passed through the sample was observed by a photomultiplier tube (R10699, Hamamatsu Photonics, Japan) equipped with a notch filter (notch-wavelength = 532 nm, NF03-532E-50×50, Semrock). The signal from the photomultiplier tube was averaged and stored in a digital-storage-oscilloscope (DPO7104, Tektronix, Japan). The obtained kinetics data were fitted by multi exponential curves individually.

ATR-FTIR Spectroscopy

ATR-FTIR spectroscopy is good at monitoring structural dynamics of proteins in aqueous solution.[11,39] Cation-binding to TaHeR was monitored by ATR-FTIR spectroscopy as described previously.[4,7,12,27] In ATR-FTIR spectroscopy, rhodopsins are normally reconstituted into lipids. However, we found that the reconstitued sample with a protein-to-lipid molar ratio of 1:20 exhibits significant protein-lipid shrinkage upon binding of divalent cations, so that ion-binding induced spectral changes were masked by absolute absorption spectra. Therefore, we did not add lipid as well as the previous study.[7] We removed the detergent with Bio-Beads (SM-2, Bio-Rad), so that TaHeR molecules are presumably surrounded by endogenous lipids.

The protein was placed on the surface of a silicon ATR crystal (Smiths, three internal total reflections) and naturally dried. The sample was then rehydrated with the buffer at a flow rate of 0.6 ml min^{-1}, and temperature was maintained at 20 °C by circulating water. The perfusion buffer is composed of 150 mM NaCl and 10 mM HEPES-Na, pH 7.0 (buffer A), to which 0.5 mM Zn^{2+} was added (buffer B). ATR‐FTIR spectra were recorded at 2 cm^{-1} resolution, using an FTIR spectrometer (Agilent) equipped with a liquid nitrogen-cooled mercury-cadmium-telluride (MCT) detector (an average of 1710 interferograms per 15 min). Cation-induced difference spectra were measured by switching buffer A and buffer B. The buffer containing the EDTA/EGTA mixture (buffer W) was perfused after Zn^{2+} perfusion to complete the removal of Zn^{2+} in the flow path, before measuring the Zn^{2+}-free form (using a flow of Zn^{2+}-free buffer). The difference spectra were calculated as the average of the presence minus absence spectra of the cation. The spectral contributions of the unbound salt, the protein-lipid swelling/shrinkage, and the water-buffer components were corrected.

MD simulation

The X-ray crystal structure of TaHeR (PDB ID: 6IS6)[4] was chosen as the initial structure. TaHeR was treated as a dimer located in the membrane environment.[4] The dimer TaHeR was placed in the lipid bilayer using membrane builder in CHARMM-GUI,[40] and then about 25000 TIP3P water molecules were also placed in the periodic box. In addition, 42 Na^+ and 48 Cl^-

ions were added to reproduce neutral cell environmental conditions. The lipid bilayer contained 60 1-palmitoyl-2-oleoyl-sn-glycero-3-phosphocholine (POPC), 60 1-palmitoyl-2-oleoyl-sn-glycero-3-phosphoethanolamine (POPE), and 30 cholesterol molecules in both upper and lower sides, respectively. For the Zn-containing system (Zn^{2+}-bound TaHeR), the initial structure in which Zn coordinating to E150 was created from the substitution of the protonated E150's proton to Zn cation. Note that 2 additional Na cations were randomly removed from the system to maintain charge neutrality. At first, energy minimization was performed, and the resultant optimized structure was used as the initial one of Zn^{2+}-bound TaHeR. The ff14SB, Lipid14, and Amber force fields were used for the amino acids, the lipids, and the atomic ions in the system, respectively.[41-43] For the retinal Schiff-base residue in the HeR, the restrained electrostatic potential (RESP) charges calculated by Gaussian 16,[44] with B3LYP-D3/Def2-TZVP level,[45-50] was applied. The force field parameters were used as the ordinary rhodopsin parameter set developed by Rothlisberger *et al.*[51]

The MD simulation and analysis were performed by the CUDA version of pmemd program in Amber 16 program package.[52-55] The trajectory of MD simulation was analyzed by cpptraj program.[56] A long-range Coulomb interaction was evaluated by using the particle mesh Ewald method with 10.0 Å cutoff in real space. The SHAKE algorithm was applied, and the time step was taken 2 fs per one step. During the dynamics, the Langevin thermostat with a collision frequency of 1 ps^{-1} was used for the temperature controlling method. The MD simulation procedure is as follows: an energy minimization, gradually increase the temperature of the system to 300 K in 400 ps, and 10 ns for equilibration at 300 K. After that, 3 μs MD simulation was performed until the averaged structure was converged.

Author contributions

H. K. conceived the project and designed the experiments. M. H. prepared samples and performed FTIR spectroscopy with the support of K. K. and Y. F. M. S. performed thermal stability and laser flash photolysis measurements. K. M., M. S. and Y. S. performed MD simulation. M. S., Y. S. and H. K. wrote the paper. All authors discussed and commented on the article.

Competing financial interests

The authors declare no competing financial interests.

Acknowledgements

This work was financially supported by grants from the Japanese Ministry of Education, Culture, Sports, Science and Technology to H.K. (18H03986, 19H04959, 21H04969) and to M.S. (22H04916), Grant-in-Aid for Scientific Research on Innovative Areas "Non-equilibrium-state molecular movies and their applications (Molecular Movies)" from MEXT, Japan (KAKENHI grant Nos. 19H05784 to Y.F.; and 20H05453 to M.S.), Grant-in-Aid for Scientific Research on Innovative Areas "Innovations for Light-Energy Conversion (I4LEC)" from MEXT, Japan (KAKENHI grant Nos. 20H05453 to M.S.), the Japan Science and Technology Agency (JST), Japan, PRESTO (grant Nos. JPMJPR19G4 to K.K.; and JPMJPR19G6 to M.S.) and CREST (grant Nos. JPMJCR1753 to H.K; and JPMJCR17N5 to Y.F.).

Keywords: rhodopsin, ATR-FTIR, transmembrane helices, retinal, molecular dynamics simulation

References

[1] O. P. Ernst, D. T. Lodowski, M. Elstner; P. Hegemann, L. S. Brown and H. Kandori, *Chem. Rev.* 2014, **114**, 126-163.

[2] A. Pushkarev, K. Inoue, S. Larom, J. Flores-Uribe, M. Singh, M. Konno, S. Tomida, S. Ito, R. Nakamura, Tsunoda, S. P. Tsunoda, A. Philosof, I. Sharon, N. Yutin, E. V. Koonin, H. Kandori and O. Béjà, *Nature* 2018, **558**, 595-599.

[3] A. Rozenberg, K. Inoue, H. Kandori and O. Béjà, *Annu. Rev. Microbiol.* 2021, **75**, 427-447.

[4] W. Shihoya, K. Inoue, M. Singh, M. Konno, S. Hososhima, K. Yamashita, K. Ikeda, A. Higuchi, T. Izume, S. Okazaki, M. Hashimoto, R. Mizutori, S. Tomida, Y. Yamauchi, R. Abe Yoshizumi, K. Katayama, S. P. Tsunoda, M. Shibata, Y. Furutani, A. Pushkarev, O. Béjà, T. Uchihashi, H. Kandori and O. Nureki, *Nature* 2019, **574**, 132-136.

[5] Y. Lu, X. E. Zhou, X. Gao, N. Wang, Xia, R. Xia, Z. Xu, Y. Leng, Y. Shi, G. Wang, K. Melcher, H. E. Xu and Y. He, *Cell Res*. 2020, **30**, 88-90.

[6] K. Kovalev, D. Volkov, R. Astashkin, A. Alekseev, I. Gushchin, J. M. Haro-Moreno, A. Rogachev, T. Balandin, V. Borshchevskiy, A. Popov, G. Bourenkov, E. Bamberg, F. Rodriguez-Valera, G. Büldt and V. Gordeliy, *Proc. Natl. Acad. Sci. U. S. A.* 2020, **117**, 4131-4141.

[7] M. Hashimoto, K. Katayama, Y. Furutani and H. Kandori, *J. Phys. Chem. Lett.* 2020, ***11***, 8604-8609.

[8] M. Singh, K. Inoue, A. Pushkarev, O. Béjà and H. Kandori, *Biochemistry* 2018, **57**, 5041-5049.

[9] M. Singh, K. Katayama, O. Béjà and H. Kandori, *Phys. Chem. Chem. Phys.* **2019**, *21*, 23663-23671.

[10] T. Tanaka, M. Singh, W. Shihoya, K. Yamashita, H. Kandori and O. Nureki, *Biochem. Biophys. Res. Commun.* 2020, **533**, 262-267.

[11] H. Kandori, *Bull. Chem. Soc. Jpn* 2020*,* **93**, 904-926.

[12] K. Katayama, Y. Furutani, M. Iwaki, T. Fukuda and H. Kandori, *Phys. Chem. Chem. Phys.* 2018, **20**, 3381-3387.

[13] Y. Kitade, Y. Furutani, N. Kamo and H. Kandori, *Biochemistry* 2009, **48**, 1595-1603.

[14] K. Inoue, H. Ono, Abe-Yoshizumi, R. Abe-Yoshizumi, S. Yoshizawa, H. Ito, Kogure, K. Kogure and H. Kandori, *Nat. Commun.* 2013, **4**, 1678.

[15] T. Fukuda, K. Muroda and H. Kandori, *Biophysics* 2013*,* **9**, 167-172.

[16] H. E. Kato, K. Inoue, R. Abe-Yoshizumi, Y. Kato, H. Ono, M. Konno, S. Hososhima, T. Ishizuka, Hoque, M. R. Hoque, H. Kunitomo, J. Ito, S. Yoshizawa, K. Yamashita, M. Takemoto, T. Nishizawa, R. Taniguchi, K. Kogure, A. D. Maturana, Y. Iino, H. Yawo, R. Ishitani, H. Kandori and O. Nureki, *Nature* 2015*,* **521**, 48-53.

[17] S. Ito, M. Iwaki, S. Sugita, R. Abe-Yoshizumi, T. Iwata, K. Inoue and Kandori, H. *J. Phys. Chem. B* 2018*,* **122**, 165-170.

[18] K. Katayama, S. Nakamura, T. Sasaki, Imai, H. Imai and H. Kandori, *Biochemistry* 2019*,* **58**, 2944-2952.

[19] T. Sugimoto, K. Katayama and H. Kandori, *J. Phys. Chem. B* 2022*,* **126**, 2203-2207.

[20] A. Rozenberg, I. Kaczmarczyk, D. Matzov, J. Vierock, T. Nagata, Sugiura, M. Sugiura, K. Katayama, Y. Kawasaki, M. Konno, Y. Nagasaka, M. Aoyama, I. Das, E. Pahima, J. Church, S. Adam, V. A Borin, A. Chazan, S. Augustin , J. Wietek, J. Dine, Y. Peleg, A. Kawanabe, Y. Fujiwara, O. Yizhar, M. Sheves, I. Schapiro, Y. Furutani, H. Kandori, K. Inoue, P. Hegemann, O. Béjà and M. Shalev-Benami, *Nat. Struct. Mol. Biol.* 2022*,* **29**, 592-603.

[21] Y. Sudo, Y. Kitade, Y. Furutani, M. Kojima, Kojima, S. Kojima, K. Homma and H. Kandori, *Biochemistry* 2009*,* **48,** 11699-11705.

[22] Y. Onoue, M. Iwaki, A, Shinobu, Y. Nishihara, H. Iwatsuki, H. Terashima, A. Kitao, H. Kandori and M. Homma, *Sci. Rep.* 2019*,* **9**, 11216.

[23] Y. Furutani, T. Murata and H. Kandori, *J. Am. Chem. Soc.* 2011*,* **133**, 2860-2863.

[24] H. Kandori, Y. Furutani and T. Murata, *Biochim. Biophys. Acta.* 2015*,* **1847**, 134-141.

[25] Y. Furutani, H. Shimizu, Y. Asai, T. Fukuda, S. Oiki and H. Kandori, *J. Phys. Chem. Lett.* 2012*,* **3**, 3806-3810.

[26] Y. Furutani, H. Shimizu, Y. Asai, S. Oiki and H. Kandori, *Biophys. Physicobiol.* 2015, **12,** 37-45.

[27] M. Iwaki, K. Takeshita, H. X. Kondo, K. Kinoshita, Y. Okamura, Y. Takano, A. Nakagawa and H. Kandori, *J. Phys. Chem. B* 2018, **122**, 9076-9080.

[28] M. Iwaki, B. Refaeli, L. Van Dijk, R. Hiller, M. Giladi, H. Kandori and D. Khananshvili, *FEBS J.* 2020*,* **287**, 4678-4695.

[29] S. Doki, H. E. Kato, N. Solcan, M. Iwaki, M. Koyama, M. Hattori, N. Iwase, T. Tsukazaki,; Y. Sugita, H. Kandori, S. Newstead, Y. Ishitani and O. Nureki, *Proc. Natl. Acad. Sci. U S A* 2013*,* **110**, 11343-11348.

[30] K. Katayama, K. Suzuki, R. Suno, H. Tsujimoto, S. Iwata, T. Kobayashi and H. Kandori, *J. Phys. Chem. Lett.* 2019*,* **10**, 7270-7276.

[31] K. Suzuki, K. Katayama, Y. Sumii, T. Nakagita, R. Suno, H. Tsujimoto, S. Iwata, T. Kobayashi, N. Shibata and H. Kandori, *RSC Adv.* 2021*,* 11, 12559-12567.

[32] K. Katayama, K. Suzuki, R. Suno, R. Kise, H. Tsujimoto, S. Iwata, A. Inoue, T. Kobayashi and H. Kandori, *Commun. Biol.* 2021*,* **4**, 1321.

[33] M. Nara, H. Torii and M. Tatsumi, *J. Phys. Chem.* 1996, **100**, 19812-19817.

[34] W. Kabsch and C. Sander, *Biopolymers* 1983, **12**, 2577-2637.

[35] S. Hososhima, R. Mizutori, R. Abe-Yoshizumi, A. Rozenberg, S. Shigemura, A. Pushkarev, M. Konno, K. Katayama, K. Inoue, S. P. Tsunoda, O. Béjà and H. Kandori, *eLife* 2022*,* **11**, e78416.

[36] S.-G. Cho, M. Song, K. Chuon, J. Shim, S. Meas and K.-H. Jung, *PLOS Biol.* 2022*,* **20**, e3001817.

[37] J.G. Shim, S.G. Cho, S.H. Kim, K. Chuon, S. Meas, A. Choi, K.-H. Jung, Microbiol. Spectr. 2022, e0221522.

[38] K. Gerwert, E. Freier, S. Wolf, *Biochim. Biophys. Acta* 2014, **1837**, 606-613.

[39] J. Güldenhaupt, T. Rudack, P. Bachler, D. Mann, G. Triola, H. Waldmann, C. Kötting, K. Gerwert, *Biophys. J.* 2012, **103**, 1585-1593.

[40] E. L. Wu, X. Cheng, S. Jo, H. Rui, K. C. Song, E. M. Dávila-Contreras, Y. Qi, J. Lee, V. Monje-Galvan, R. M. Venable, J. B. Klauda and W. Im, *J. Comput. Chem.* 2014, **35**, 1997-2004.

[41] J. A. Maier, C. Martinez, K. Kasavajhala, L. Wickstrom, K. E. Hauser, Simmerling and C. Simmerling, *J. Chem. Theory Comput.* 2015, **11**, 3696-3713.

[42] C. J. Dickson, B. D. Madej, Skjevik, Å. A. Skjevik, Betz, R. M. Betz, K. Teigen, I. R. Gould and R. C. Walker, *J. Chem. Theory Comput.* 2014, **10**, 865-879.

[43] J. W. Ponder, and D. A. Case, *Adv. Protein Chem.* 2003, **66**, 27-85.

[44] M. J. Frisch, G. W. Trucks, H. B. Schlegel, G. E. Scuseria, M. A. Robb, J. R. Cheeseman, G. Scalmani, V. Barone, G. A. Petersson, H. Li, X. Nakatsuji, M. Caricato, A. V. Marenich, J. Bloino, B. G. Janesko, R. Gomperts, B. Mennucci, H. P. Hratchian, J. V. Ortiz, A. F. Izmaylov, J. L. Sonnenberg, D. Williams-Young, F. Ding, F. Lipparini, F. Egidi, J. Goings, B. Peng, A. Petrone, T. Henderson, D. Ranasinghe, V. G. Zakrzewski, J. Gao, N. Rega, G. Zheng, W. Liang, M. Hada, M. Ehara, K. Toyota, R. Fukuda, J. Hasegawa, M. Ishida, T. Nakajima, Y. Honda, O. Kitao, H. Nakai, T. Vreven, K. Throssell, J. A. Montgomery, Jr., J. E. Peralta, F. Ogliaro, M. J. Bearpark, J. J. Heyd, E. N. Brothers, K. N. Kudin, V. N. Staroverov, T. A. Keith, R. Kobayashi, J. Normand, K. Raghavachari, A. P. Rendell, J. C. Burant, S. S. Iyengar, J. Tomasi, M. Cossi, J. M. Millam, M. Klene, C. Adamo, R. Cammi,

J. W. Ochterski, R. L. Martin, K. Morokuma, O. Farkas, J. B. Foresman, and D. J. Fox, *Gaussian, Inc., Wallingford CT,* 2016.

[45] A. D. Becke, *J. Chem. Phys.* 1993, **98**, 5648-5652.

[46] S. H. Vosko, L. Wilk and M. Nusair, *Can. J. Phys.* 1980, **58**, 1200-1211.

[47] C. Lee, W. Yang, Parr and R. G. Parr, *Phys. Rev. B* 1988, **37**, 785-789.

[48] P. J. Stephens, F. J. Devlin, C. F. Chabalowski and M. J. Frisch, *J. Phys. Chem.* 1994, **98**, 11623-11627.

[49] S. Grimme, J. Antony, S. Ehrlich and H. Kreig, *J. Chem. Phys.* 2010, **132**, 154104.

[50] F. Weigend and R. Ahlrchs, *Phys. Chem. Chem. Phys.* 2005, **7**, 3297-3305.

[51] M. Doemer, P. Mauer, P. Campomanes, I. Tavarnelli and U. Rothlisberger, *J. Chem. Theory Comput.* 2014, **10,** 412-422.

[52] D. A. Case, T. E. Cheatham III, T. Darden, H. Gohlke, R. Luo, Merz, K. M. Jr. Merz, A. Onufriev, Simmerling, C. Simmerling, B. Wang and R. J. Woods, *J. Comput. Chem.* 2005, **26**, 1668-1688.

[53] A. W. Götz, M. J. Williamson, D. Xu, D. Poole, Grand, S. Le Grand and R. C. Walker, *J. Chem. Theory Comput.* 2012, **8**, 1542-1555.

[54] R. Salomon-Ferrer, A. W. Götz, D. Poole, S. Le Grand and R. C. Walker, *J. Chem. Theory Comput.* 2013, **9,** 3878-3888.

[55] S. Le Grand, A. W. Götz and R. C. Walker, *Comput. Phys. Commun.* 2013, **184**, 374-380.

[56] D. R. Roe and T. E. Cheatham III *J. Chem. Theory Comput.* 2013, **9**, 3084-3095.

Figures

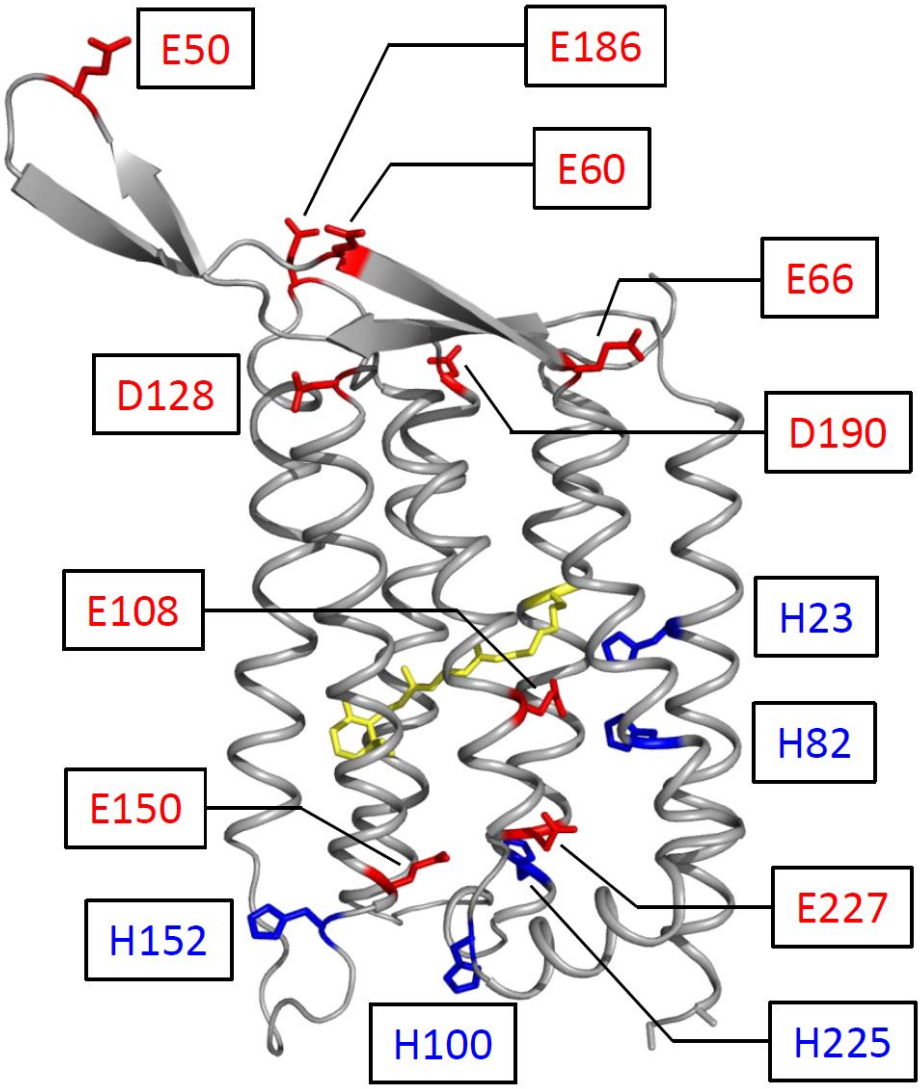

Figure 1. Location of glutamates, aspartates, and histidines in TaHeR. Top and bottom sides correspond to the C-terminal and N-terminal sides that face the extracellular and cytoplasmic region, respectively.

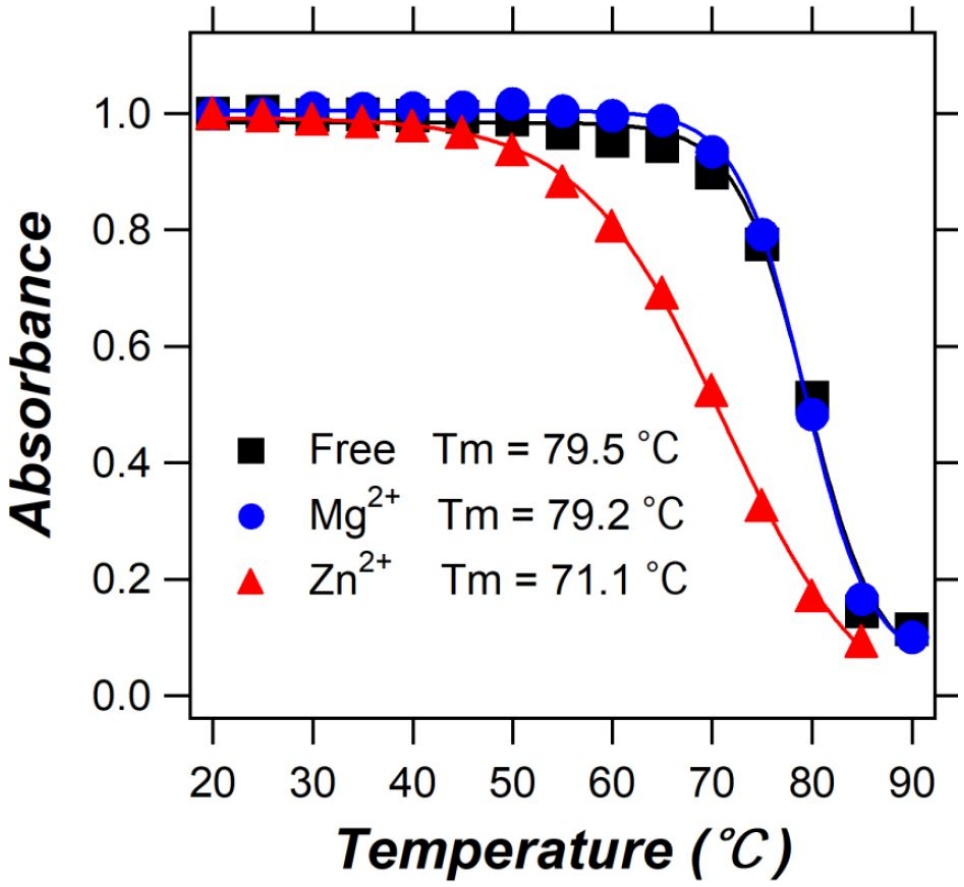

Figure 2. Thermal stability of TaHeR in the absence of divalent cations (black), and presence of 0.5 mM Mg^{2+} (blue) or Zn^{2+} (red). The absorbance is measured at 542 nm, and the samples are kept for 5 min at each temperature before the measurements.

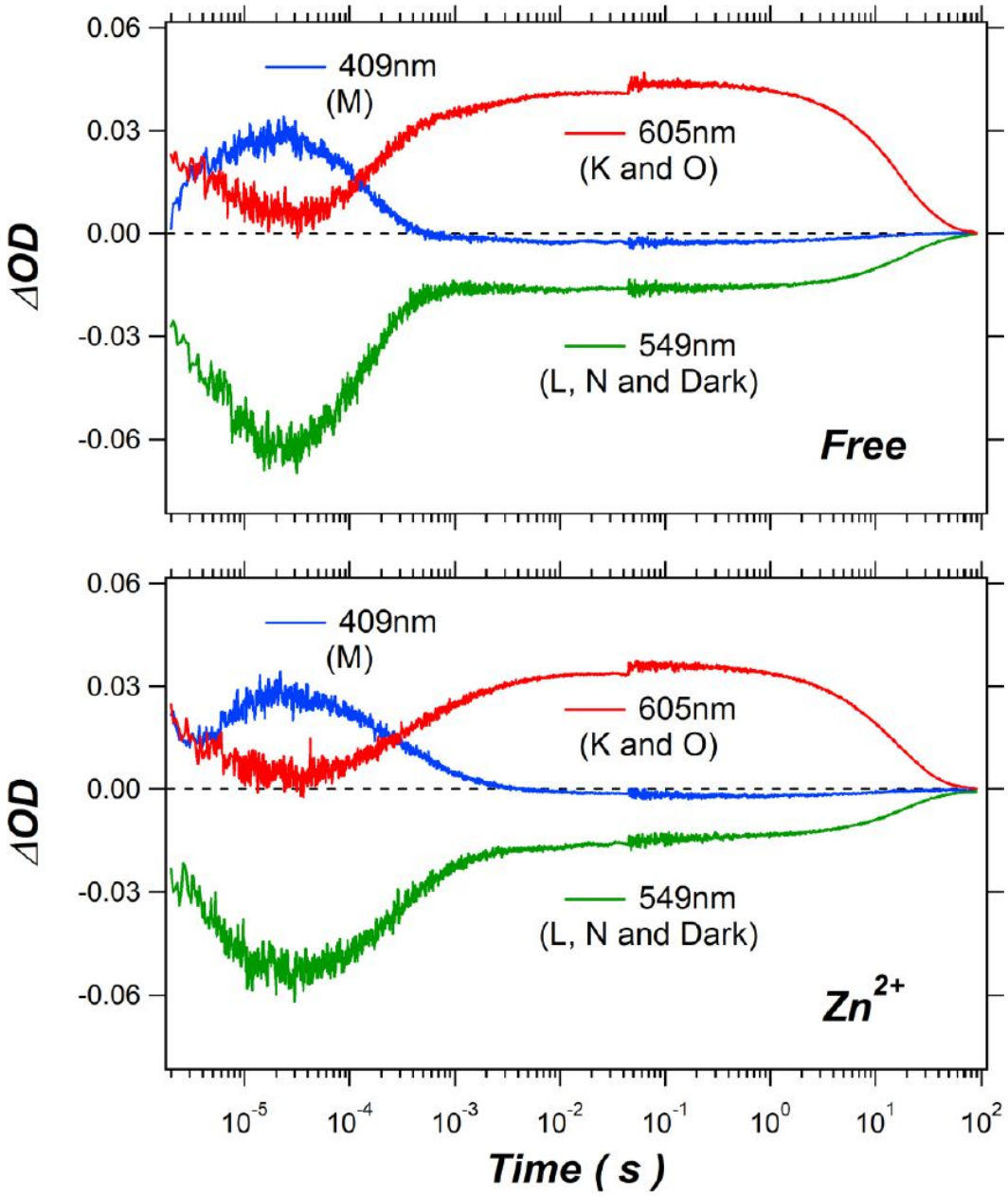

Figure 3. Kinetic changes of TaHeR at 409, 549, and 605 nm in the absence (upper panel) and presence (lower panel) of 0.5 mM Zn^{2+}.

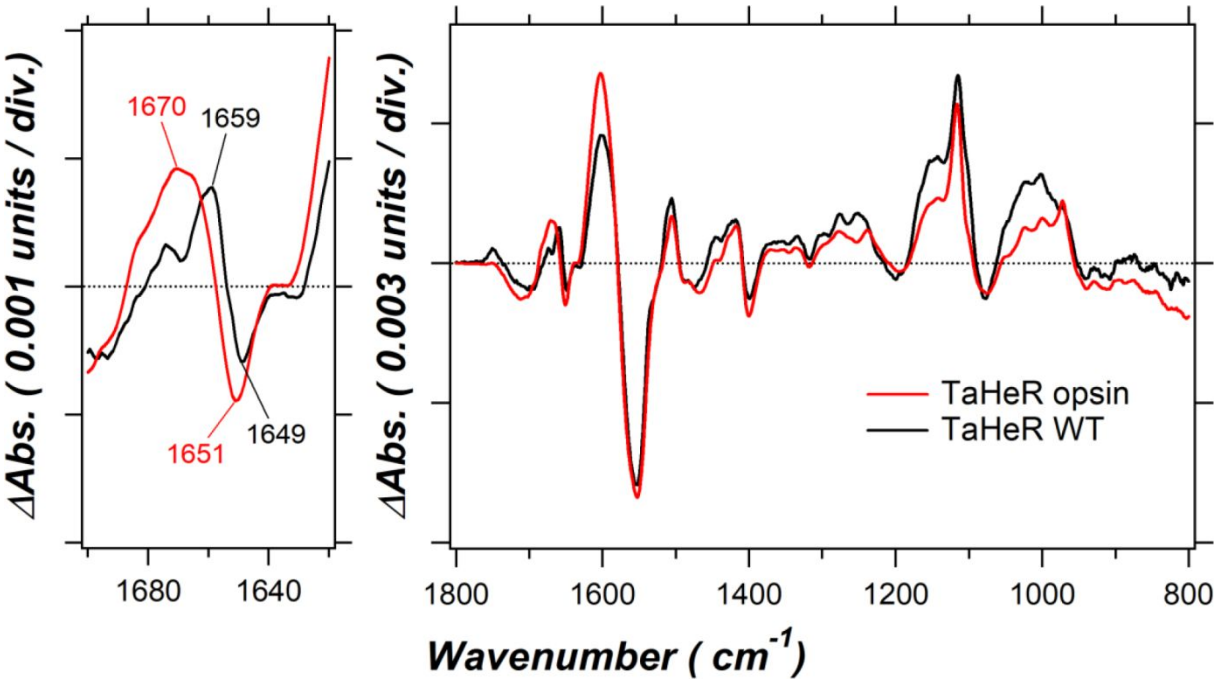

Figure 4. Difference ATR-FTIR spectra for TaHeR (black) and TaHeR opsin (red). Positive and negative signals represent the measurements in the presence and absence of 0.5 mM Zn^{2+}, respectively.

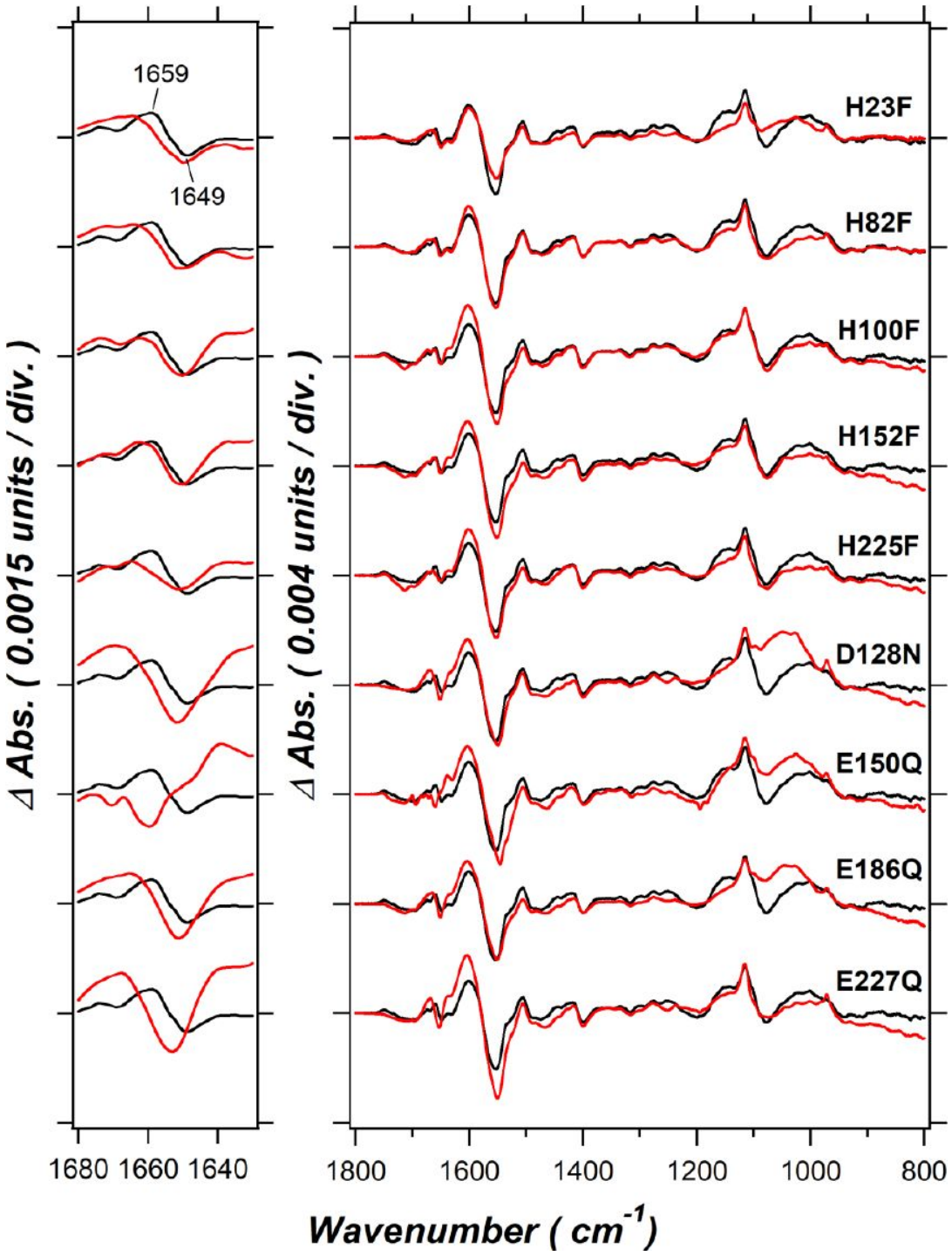

Figure 5. Difference ATR-FTIR spectra for TaHeR (black) and TaHeR mutants (red). Positive and negative signals represent the measurements in the presence and absence of 0.5 mM Zn^{2+}, respectively.

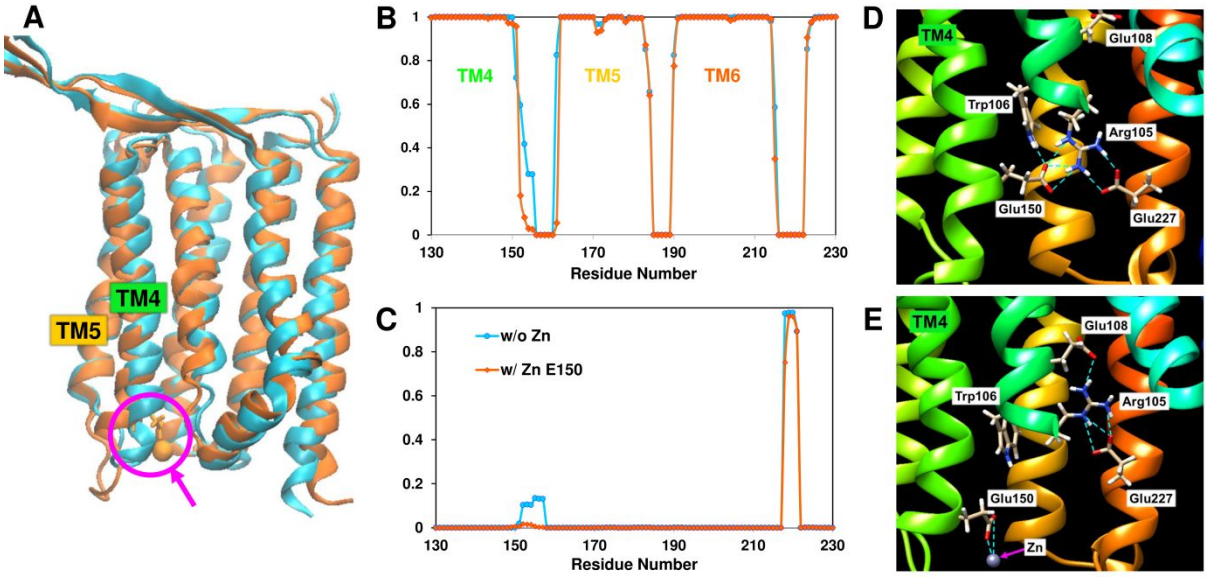

Figure 6. (A) The overlayed representative structure of natural TaHeR (blue) and Zn^{2+} coordinated TaHeR (orange). The Zn^{2+} and E150 is highlighted by pink circle and arrow. (B) Alpha-helix and (C) 3-10 helix structure distribution during the MD simulation. The blue and orange lines indicate TaHeR and Zn^{2+}-bound TaHeR, respectively. (D) The hydrogen bonding network nearby E150 for TaHeR and (E) that for Zn^{2+}-bound TaHeR.

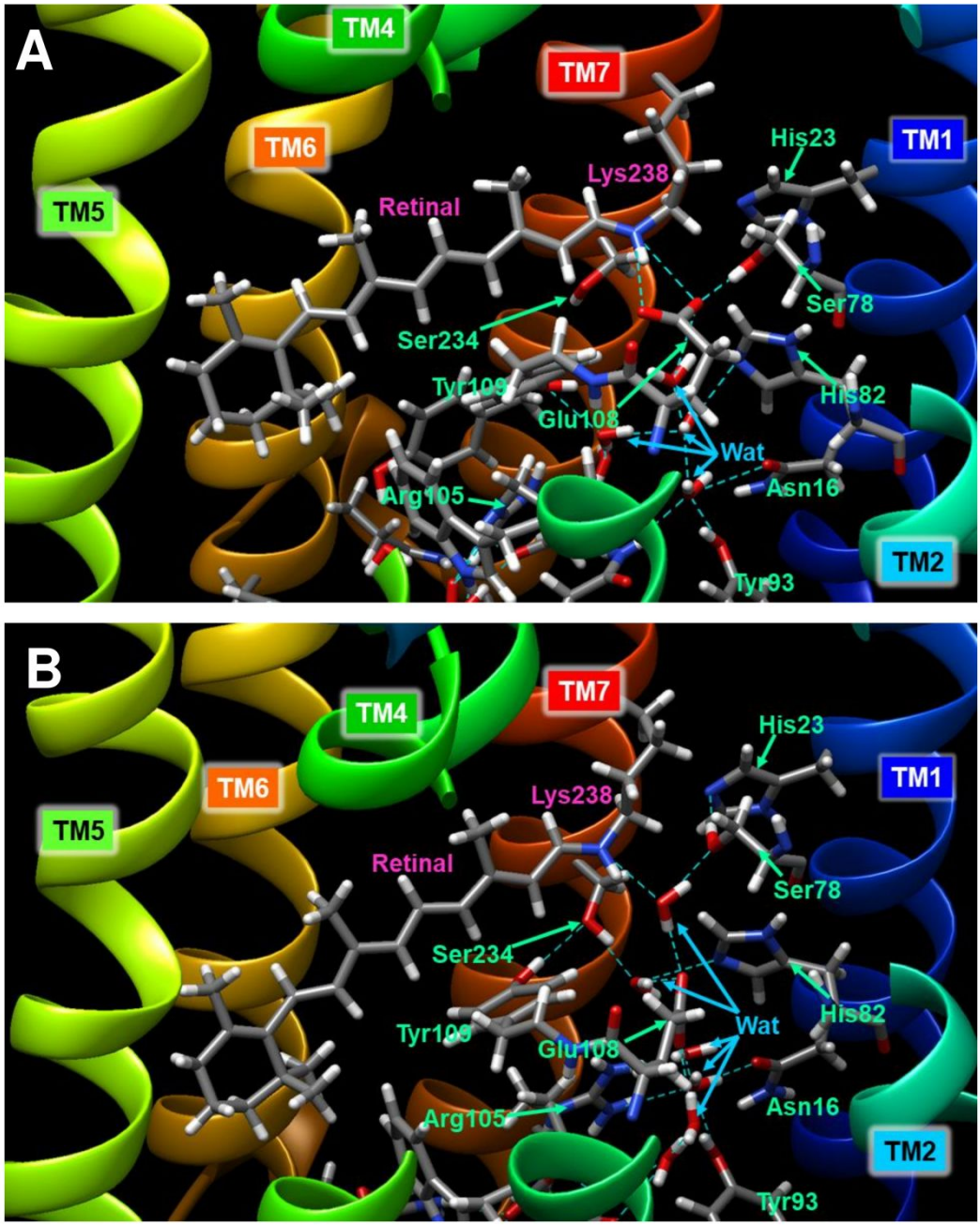

Figure 7. (A) The hydrogen bonding network nearby the retinal Schiff base for TaHeR and (B) that for Zn^{2+}-bound TaHeR, respectively. Some portions of TM*n* structures were omitted to show the retinal clearly.